A PARALLEL IMPLICITLY COUPLED FLUID-STRUCTURE INTERACTION ALGORITHM FOR BLOOD FLOW IN ARTERIES

ANDREW T. BARKER AND XIAO-CHUAN CAI

Abstract. We develop a scalable parallel finite element solver for the simulation of blood flow in compliant arteries. The incompressible Navier-Stokes equations are solved for the fluid and coupled to a linear elastic model for the blood vessel walls. Our solver features an unstructured dynamic mesh capable of modeling complicated geometries, an arbitrary Lagrangian-Eulerian framework that allows for large displacements of the fluid domain, and fully implicit monolithic coupling between the fluid and structure equations. A scalable and robust parallel Newton-Krylov-Schwarz method is used to solve the resulting systems of coupled nonlinear equations.

1. Introduction

Artery disease is the leading cause of death in developed nations, and by some accounts is the leading cause of death worldwide [12]. Artery disease is closely associated with flow properties of the blood and with the interaction between the blood and the vessel wall. In particular, areas of turublence, flow recirculation, or places where the artery wall is subject to low or oscillating shear stress are at higher risk for plaque formation and disease. Accurate modeling of these flow characteristics might enable better prediction of when and where artery disease will occur and lead to more accurate, less invasive, and more timely treatment.

Very often in the simulation of fluid-structure interaction, the coupling between the fluid and the structure is done iteratively. That is, first a fluid problem is solved with some boundary conditions; then, the solution to this problem is used to assign boundary conditions for the structure. The structure solution in turn provides improved boundary conditions for the fluid problem, and this iterative process is continued until the boundary conditions are changing little enough that they can be considered compatible at the fluid-structure interface [7], [10], [16]. However, this approach can become unstable, requiring the use of impractically small timesteps, and can reduce the order of accuracy of the solution [11]. In contrast, we use fully monolithic coupling, where the fluid and the structure are solved together as one system.

As a particular example of fluid-structure interaction, blood flow simulation has attracted a great deal of attention. We mention only a few recent papers. In [3], [5], [6], and [17], coupled fluid-structure problems are solved in 3D for patient-specific artery models. These papers pay a great deal of attention to accurately representing vessel geometry, to the consitutive model for the artery walls, and to finding the correct boundary conditions to apply at the outlet. Some of them do monolithic coupling of fluid and structure and some parallel processing. But none of these papers report specifically on the parallel performance and scalability of their algorithms, and none does truly large-scale computation.

Our interest in this paper is in developing a framework for scalable parallel algorithms for this problem, so at this point certain parts of our model are physically unrealistic. In particular, all our simulations are 2D, we model artery walls as a linear elastic solid, and our outlet boundary

Andrew T. Barker, Department of Applied Mathematics, University of Colorado, Boulder, Colorado 80309-0526, andrew.barker@colorado.edu.

Xiao-Chuan Cai, Department of Computer Science, Univeristy of Colorado, Boulder, Colorado 80309-0430, cai@cs.colorado.edu.

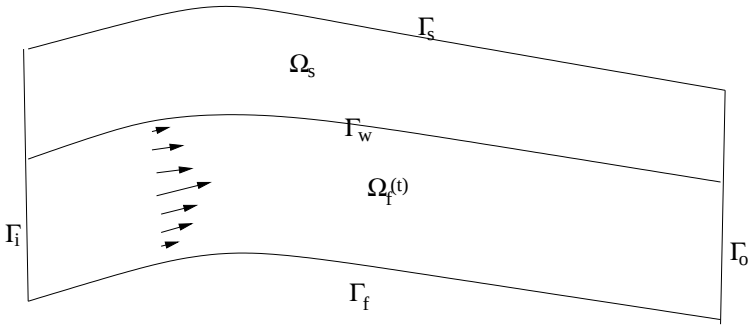

FIGURE 1. Ω_0 is the reference configuration of the fluid domain and $\Omega_f(t)$ represents the moving fluid domain at time t; Ω_s is the structure domain in the reference (Lagrangian) configuration. Γ_i and Γ_o are the inlet and outlet boundaries, respectively, to the fluid domain and Γ_f is the rigid (no-slip) wall to the fluid domain, while Γ_s is the dry boundary to the structure, and Γ_w is the wet fluid-structure interaction surface.

conditions are simplistic. But we demonstrate that our method has attractive convergence properties and good scalability, and even at this stage we can qualitatively reproduce some of the more important aspects of blood flow in compliant arteries.

We restrict our attention to large blood vessels, where the fluid properties are approximately Newtonian, and model with the incompressible Navier-Stokes equations. To account for the moving fluid domain, we use a time-dependent computational mesh in the arbitrary Lagrangian-Eulerian (ALE) framework [4]. We solve the fully time-dependent and nonlinear equations with implicit coupling of the three components: the fluid, the elastic wall structure, and the moving mesh. See Figure 1 for a schematic and some notation.

2. Governing equations

2.1. **Structure equations.** We use a linear elastic model for the structure as in [15]. The primary variable in the structure equations is the displacement vector $\mathbf{x}_s = (x_1\ x_2)^T$. Define σ_s as the stress-strain relation or Cauchy stress tensor

$$\sigma_s = \lambda_s(\nabla \cdot \mathbf{x}_s)I + 2\mu_s(\nabla \mathbf{x}_s + \nabla \mathbf{x}_s^T)$$

where λ_s and μ_s are the Lamé constants which are a property of the physical material under consideration. The Lamé parameters are related to the Young's modulus E and the Poisson ratio ν_s by

$$\lambda_s = \frac{\nu_s E}{(1+\nu_s)(1-2\nu_s)}, \qquad \mu_s = \frac{E}{2(1+\nu_s)}.$$

The equilibrium equation for linear elasticity is

$$\rho_s \frac{\partial^2}{\partial t^2}\mathbf{x}_s = \nabla \cdot \sigma_s + \mathbf{f}_s. \tag{1}$$

We also need to specify boundary and initial conditions. We fix the structure displacement $\mathbf{x}_s = 0$ on Γ_S. The boundary conditions on Γ_w will be discussed when we discuss the fluid-structure coupling.

2.2. **Moving mesh.** The mesh points of our fluid domain move, and the displacements of the mesh nodes from their original reference configuration make a separate field that we need to represent. For the grid displacements $\mathbf{x}_f$, we simply use the Laplace equation

$$\Delta \mathbf{x}_f = 0 \tag{2}$$

on the interior of the domain, following [13]. In our numerical simulations this simple relation gives a smooth grid as the boundaries of the domain move, rarely causing problems with ill-conditioned elements. The boundary conditions for this field are either fixed zero Dirichlet conditions (at the inlet and outlet of the fluid domain) or are prescribed to follow the movement of the structure.

2.3. **Fluid equations.** We model blood as a viscous incompressible Newtonian fluid, using the Navier-Stokes equations written in the ALE frame

$$\left.\frac{\partial \mathbf{u}_f}{\partial t}\right|_Y + [(\mathbf{u}_f - \omega_g)\cdot\nabla]\mathbf{u}_f + \frac{1}{\rho_f}\nabla p = \nu_f \Delta \mathbf{u}_f \tag{3}$$

$$\nabla \cdot \mathbf{u}_f = 0. \tag{4}$$

Here $\mathbf{u}_f$ is the fluid velocity vector and p is the pressure. The given data include the fluid density ρ_f, $\nu_f = \mu_f/\rho_f$ which is the kinematic viscosity. External body forces are ignored. Also, $\omega_g = \partial \mathbf{x}_f/\partial t$ is the velocity of the moving mesh in the ALE frame and the Y indicates that the time derivative is to be taken with respect to the ALE coordinates, not the Eulerian coordinates [13].

Boundary conditions for the fluid equations consist of a no-slip condition $\mathbf{u}_f = 0$ at rigid walls Γ_f, a Dirichlet condition where $\mathbf{u}_f$ takes a given profile at the inlet Γ_i, and a zero traction condition

$$\sigma_f \cdot \mathbf{n} = \nu_f(\nabla \mathbf{u}_f \cdot \mathbf{n}) - p\mathbf{n} = 0 \tag{5}$$

on the outlet Γ_o, where σ_f is the Cauchy stress tensor for the fluid and $\mathbf{n}$ is the unit outward normal. The boundary conditions on Γ_w will be discussed in the next section.

2.4. **Fluid-structure coupling.** At the fluid-structure boundary we require that structure velocity match fluid velocity $\mathbf{u}_f = \partial \mathbf{x}_s/\partial t$ and also we enforce that the moving mesh must follow the solid movement $\mathbf{x}_f = \mathbf{x}_s$, so that the solid can maintain a Lagrangian description.

The most difficult part of the fluid coupling is the coupling of so-called traction forces at the boundary. This can be written $\sigma_s \cdot \mathbf{n} = \sigma_f \cdot \mathbf{n}$ where $\mathbf{n}$ is the unit normal vector at the fluid-solid interface and σ_s and σ_f are the Cauchy stress tensors for the solid and fluid, respectively. This traction condition is enforced as a Neumann-type boundary condition on the structure equations.

3. Spatial discretization

Because of space constraints, we omit the full derivation of the weak form of the governing equations. This development is standard, multiplying the strong form by test functions and integration by parts. We note two interesting points here.

First, because of our moving grid, the variational spaces in which we seek a solution to the fluid subproblem is time-dependent. The velocity space is a subspace of $[H^1(\Omega_f(t))]^2$, and the pressure space belongs to $L^2(\Omega_f(t))$. Second, the variational spaces (and corresponding discretized finite element spaces) associated with the fluid subproblem and the mesh subproblem depend implicitly on the current solution to the structure subproblem, as this solution provides essential boundary conditions for the fluid and mesh subproblems.

All the spatial discretization is done with quadrilateral finite elements, with conforming discretization at the fluid-structure interface, so that no special interpolation scheme is necessary to move information between fluid and structure.

3.1. **Structure equations.** We discretize the structure using biquadratic Q_2 quadrilateral finite elements. We write the displacement vector $\mathbf{x}_s$ as a finite-dimensional approximation $\mathbf{x}_s \approx \sum_j \phi_j(x) x_j(t)$ where the ϕ_j are the finite element basis functions. We will denote the vector of coefficients x_j as x_s. Using this approximation, we arrive at the semi-discrete system of ODEs

$$M_s \frac{d^2}{dt^2} x_s + K_s x_s = F. \tag{6}$$

In practice we add a Rayleigh damping matrix (see [9]) so that (6) becomes

$$M_s \frac{d^2}{dt^2} x_s + C_s \frac{d}{dt} x_s + K_s x_s = F \tag{7}$$

where $C_s = \alpha M_s + \beta K_s$ where α and β are small parameters; typically $\alpha \approx 0.1$ and $\beta \approx 0.01$.

3.2. **Moving mesh.** We use Q_2 finite elements in our ALE discretization of the moving mesh. We approximate $\mathbf{x}_f \approx \sum_j \xi_j(x) x_j(t)$. This is a standard finite-element discretization of the Laplace equation resulting in $K_m x_f = 0$ with boundary conditions that depend on the structure subproblem.

3.3. **Fluid equations.** We use $Q_2 - Q_1$ finite elements to discretize the fluid. Using finite-dimensional approximations

$$\mathbf{u}_f \approx \sum_j \phi_j(x,t) u_j(t), \qquad p \approx \sum_j \psi_j(x,t) p_j(t)$$

we can write the semi-discrete Navier-Stokes equations in the ALE frame as

$$M_f \frac{d}{dt} u + B(u)u + K_f u - Q^T p = M_f f \tag{8}$$

$$Qu = 0 \tag{9}$$

where M_f is a mass matrix, $B(u)$ represents the nonlinear convective operator, K_f is the discrete Laplacian, and Q is the discrete divergence operator.

3.4. **Fluid-structure coupling.** The mesh displacement continuity and velocity continuity conditions are enforced directly at each timestep; we replace rows of the matrix corresponding to these degrees of freedom with rows of the form $[0 \quad 0 \cdots 1 \cdots 0 \cdots -1 \cdots 0 \quad \cdots]$, that is $x_s = x_f$, and similarly for the velocity.

It takes more work to discretize the fluid-structure traction condition. We need to discretize the force that the fluid exerts on the solid boundary, namely $\sigma_f \cdot \mathbf{n}$. The x component of this force is

$$-\sum_j p_j \int \psi_j \phi_k n_1 + 2\mu_f \left[\sum_j u_j \int \frac{\partial \phi_j}{\partial x} \phi_k n_1 \right] + \mu_f \left[\sum_j u_j \int \frac{\partial \phi_j}{\partial y} \phi_k n_2 + \sum_j v_j \int \frac{\partial \phi_j}{\partial x} \phi_k n_2 \right]$$

and similarly for the y component. These correspond to the block matrix equation

$$\sigma_f \cdot \mathbf{n} = \begin{pmatrix} A_{uu} & A_{uv} & A_{up} \\ A_{vu} & A_{vv} & A_{vp} \end{pmatrix} \begin{pmatrix} u_f \\ v_f \\ p \end{pmatrix} = (A_u \; A_p) \begin{pmatrix} u \\ p \end{pmatrix}. \tag{10}$$

This will be inserted as a force in the discrete form of the structure equations to enforce the traction matching condition at the fluid-structure interface.

4. Temporal discretization

We use the trapezoid rule $y^{n+1} = y^n + (\Delta t/2)\left(f^{n+1} + f^n\right)$ which is a second-order accurate implicit scheme for all our time discretization.

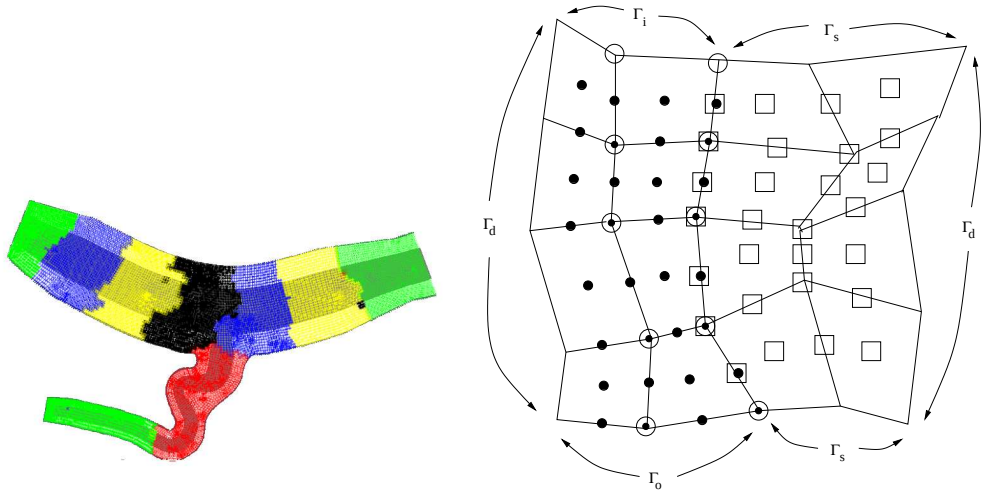

FIGURE 2. (left) An example of the mesh partitioning. The portions of the mesh assigned to different processors are in different colors, and the background shading is different for the fluid and the structure parts of the mesh. The partitioning algorithm does not consider whether the elements are fluid or structure. (right) Boundary conditions for a subdomain problem. (•) respresents a fluid velocity degree of freedom, (○) is pressure, and (□) is structure displacement.

4.1. **Structure equations.** For the structure time-stepping, we follow [9] in implementing the trapezoid rule (a special case of the Newmark method) by reducing the order of (7) from second order to first order. Our new vector of unkowns includes both solid displacement and velocity, $y = (x_s, \dot{x}_s)^T$. Then

$$\dot{y} = f(y,t) = \begin{pmatrix} \dot{x_s} \\ M^{-1}(F(t) - K_s x_s - C_s \dot{x_s}) \end{pmatrix}.$$

The trapezoid rule for this differential algebraic equation can be written

$$My^{n+1} = My^n + \frac{\Delta t}{2}\left[Ky^{n+1} + Ky^n + F^{n+1} + F^n\right]$$

where

$$M = \begin{pmatrix} I & \\ & M_s \end{pmatrix}, \quad K = \begin{pmatrix} & I \\ -K_s & -C_s \end{pmatrix}.$$

4.2. **Moving mesh.** The moving mesh, like the continuity equation for the fluid, is enforced independent of time. So we simply require

$$K_m x_f^{n+1} = 0$$

at each time step.

4.3. **Fluid equations.** Rewriting (8) in the form $u' = f(u)$ we have

$$\frac{d}{dt}u = -M_f^{-1}B(u)u - M_f^{-1}K_f u + M_f^{-1}Q^T p + f.$$

A straightforward application of the trapezoid rule would give us

$$(M + W)u^{n+1} = Mu^n + \frac{\Delta t}{2}\left[R^{n+1}u^{n+1} + R^n u^n\right]$$

where

$$M = \begin{pmatrix} M_f & 0 \\ 0 & 0 \end{pmatrix}, \quad W = \begin{pmatrix} 0 & 0 \\ Q & 0 \end{pmatrix}, \quad R^n = \begin{pmatrix} -B(u^n) - K_f & Q^T \\ 0 & 0 \end{pmatrix}.$$

This formulation, though, leads to spurious pressure oscillations, so we instead follow [8] and have

$$M = \begin{pmatrix} M_f & 0 \\ 0 & 0 \end{pmatrix}, \quad W = \begin{pmatrix} 0 & -\Delta t Q^T \\ Q & 0 \end{pmatrix}, \quad R^n = \begin{pmatrix} -B(u^n) - K_f & 0 \\ 0 & 0 \end{pmatrix}.$$

This makes sense if we think of pressure as entirely a scalar variable with no time component.

4.4. **Fluid-structure coupling.** We use the same time-stepping scheme for fluid and structure, so we can simply enforce the coupling at each timestep. In summary, we have

$$(M+W)y^{n+1} - My^n - \frac{\Delta t}{2}(Ky^{n+1} + Ky^n) - \frac{\Delta t}{2}(F^{n+1} + F^n) = 0 \tag{11}$$

where

$$y = \begin{pmatrix} u^{n+1} \\ p^{n+1} \\ x_f^{n+1} \\ x_s^{n+1} \\ \dot{x_s}^{n+1} \end{pmatrix}, \quad M = \begin{pmatrix} M_f & & & \\ & & & \\ & & I & \\ & & & M_s \end{pmatrix},$$

$$W = \begin{pmatrix} & -\Delta t Q^T & & \\ Q & & & \\ & & K_m & \\ A_u & A_p & & \\ & & & \end{pmatrix}, \quad K = \begin{pmatrix} -B - K_f & & & \\ & & & \\ & & & I \\ & & -K_s & -C_s \end{pmatrix}.$$

Though written in matrix form, many of the operators above are nonlinear. In particular the B term depends on u_f, and the K_f, M_f and Q terms depend on the moving mesh x_f. This implies that we have a Jacobian of the form

$$J = \begin{pmatrix} J_f & -\Delta t Q^T & Z_m & & \\ Q & & Z_c & & \\ & & K_m & & \\ A_u & A_p & & I & -(\Delta t/2)I \\ & & & (\Delta t/2)K_s & M_s + (\Delta t/2)C_s \end{pmatrix} \tag{12}$$

where J_f is the Jacobian of the nonlinear term in the momentum equation and Z_m and Z_c are the nonlinear contribution of the moving mesh to the momentum and continuity equations. The form of Z_m and Z_c are unknown, and our implementation of the Jacobian simply ignores them, which is a reasonable approximation as long as the mesh movement is slow—that is, the timestep is sufficiently small.

5. Solving the nonlinear system

5.1. **One level Newton-Krylov-Schwarz.** At each timestep, we solve the nonlinear system (11) with an inexact Newton method with line search. At each Newton step we solve a preconditioned linear system of the form $J(y)M^{-1}(Ms) = z$ for the Newton correction s, where M^{-1} is a one-level additive Schwarz preconditioner [14]. To formally define M^{-1}, we first partition the entire domain Ω into non-overlapping subdomains $\Omega_\ell, \ell = 1, \ldots, N$. Then each subdomain Ω_ℓ is extended to overlap its neighbors, with the overlapping domains denoted Ω'_ℓ. The domain decomposition and extension respects element boundaries, so that each Ω_ℓ and Ω'_ℓ consists of an integral number of finite elements, but subdomains do not consider the fluid-structure boundary, so that a subdomain man contain fluid elements, structure elements, or both (see Figure 2). A parameter δ represents

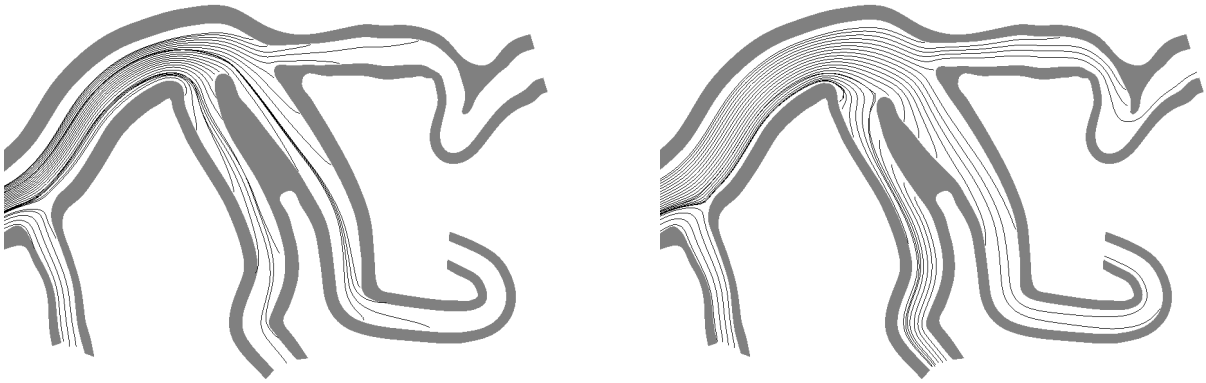

FIGURE 3. The image on the left is near the initial, unstressed configuration, and the figure on the right is at simulation time $t = 6.0$ s. Note the compression of the walls in response to fluid force.

the size of the overlap in terms of number of elements. Subdomains on a physical boundary are not extended.

On each subdomain Ω'_ℓ we construct a subdomain preconditioner B_ℓ whose elements are $B_\ell^{i,j} = J_{ij}$, where the node indexed by (i, j) is in the corresponding subdomain Ω'_ℓ. Homogeneous Dirichlet boundary conditions are used on the subdomain boundaries Γ_d for all solution variables, including fluid pressure; see Figure 2. The additive Schwarz preconditioner can be written as

$$M^{-1} = (R_1)^T B_1^{-1} R_1 + \cdots + (R_N)^T B_N^{-1} R_N.$$

If n is the total number of unknowns in Ω and n'_ℓ is the number of unknowns in Ω'_ℓ, then R_ℓ is an $n'_\ell \times n$ restriction matrix which maps the global vector of unkowns to those belonging to a subdomain. Various inexact additive Schwarz preconditioners can be constructed by replacing the matrices B_ℓ above with convenient or inexpensive to compute matrices. In our algorithm we use LU factorization for the subdomain preconditioner.

5.2. **Ordering of unknowns.** In practice, we order the unknowns for the Jacobian system not by field ordering as in (12), but by element ordering. The choice of ordering can have significant effect on the convergence properties of the solver. By choosing element ordering, the nonzero-block structure is banded. That is, within each element the unknowns are ordered as in (12), but globally the matrix looks like the nine-point stencil for a Poisson equation.

6. Numerical Results

Our solver is implemented using the Portable Extensible Toolkit for Scientific Computing (PETSc) [1], [2]. All computations are performed on an IBM BlueGene/L supercomputer at the National Center for Atmospheric Research with 1024 compute nodes.

It is important to impose initial conditions that are compatible at the fluid-structure interface. Since we begin all our simulations with zero initial conditions for structure displacement and fluid velocity, this compatibility is easily satisfied. In all the numerical results in this paper, we use a timestep $\Delta t = 0.01$, a Young's modulus $E = 1.0 \cdot 10^5$, we stop the linear solver when the preconditioned residual has decreased by a factor of 10^{-4} and we stop the Newton iteration when the nonlinear residual has decreased by a factor of 10^{-6}. We set GMRES to restart every 40

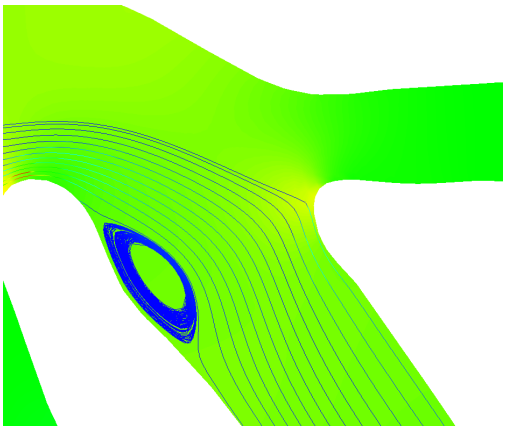

FIGURE 4. Close up of a recirculation vortex in a blood-flow simulation. This simulation has stiff artery walls (no slip conditions on the fluid) so there is no fluid-structure interaction.

iterations, and have the structural damping parameters $\alpha = 0.1, \beta = 0.01$. For all our simulations we start with zero initial conditions and proceed 10 timesteps, reporting average walltime and nonlinear iteration count per timestep, and average GMRES iterations per Newton step.

It is important in fluid-structure interaction simulation to be able to deal with large deformation of the computational grid without the quality of the mesh degrading and affecting convergence. Our simulations seem to fit this criterion; see Figure 3, where the simulation continues even after quite large changes in the shape and position of an artery wall. As in any fluid dynamics simulation, in the blood flow problem it is useful to be able to resolve vortices and other interesting features of the flow. Our simulations have sufficient spatial resolution to do this; see Figure 4.

The scalability of our algorithm is presented in Table 1. Our method scales well with respect to number of processors and scales fairly well with respect to problem size. It is also worth noting the large grid sizes and processor counts that we have used with success. The growth in GMRES iterations for large processor counts suggests that less than perfect speedup could probably be improved by use of a multilevel preconditioner.

Our simulation is also robust with respect to physical parameters. In Table 2, we show numerical results for various Reynolds numbers. Many blood flow simulations, for example [3], use Reynolds numbers in the range 30–100, but we can exceed that without much difficulty. As the Poisson ratio ν_s approaches 1/2 the structure becomes incompressible and the structure problem becomes more numerically challenging. This effect is apparent in Table 3, where $\nu_s = 0.49$ corresponds to significantly longer runtimes, but our code can still simulate this case correctly. In [3], $\nu_s = 0.3$ is used for artery walls.

7. Conclusion

Accurate modeling of blood flow in compliant arteries is a computational challenge. In order to meet this challenge, we need not only to model the physics accurately but also to develop scalable algorithms for parallel computing. In this paper we develop a Newton-Krylov-Schwarz solver that scales well in parallel and is effective for solving the implicitly coupled fluid-structure interaction problem. Our method is quite robust with respect to different vessel geometries, Reynolds numbers, Poisson ratios, spatial mesh sizes and time step sizes.

Future work will achieve more accurate results by using a more complicated, nonlinear structural model. Our solver is already fully nonlinear, so this improvement should not be too difficult. In

unknowns	np	GMRES	Newton	time
	64	9.3	5.0	123.44
$1.0 \cdot 10^6$	128	13.4	5.0	57.11
	256	18.2	5.0	36.41
	512	24.0	5.0	22.08
	128	17.5	4.8	125.31
	256	21.5	4.8	66.11
$2.1 \cdot 10^6$	512	29.7	4.8	39.97
	1024	35.9	4.8	22.90
	2048	40.0	4.8	17.25
	128	15.1	4.7	198.34
	256	20.1	4.7	100.23
$2.6 \cdot 10^6$	512	29.3	4.7	46.50
	1024	40.0	4.7	28.11
	2048	48.6	4.7	21.10

TABLE 1. Speedup and scalability. In this table ASM overlap $\delta = 2$, Reynolds number = 132.02, $\nu_s = 0.30$.

unknowns	np	Re	GMRES	Newton	time
	256	33.00	12.0	4.8	187.34
	256	66.01	12.1	4.8	184.70
$2.1 \cdot 10^6$	256	132.02	12.2	4.8	184.44
	256	264.03	12.5	4.8	188.16
	256	1056.12	12.7	10.0	385.27
	256	33.00	12.9	4.7	216.14
	256	66.01	13.1	4.7	215.95
$2.6 \cdot 10^6$	256	132.02	13.5	4.7	216.15
	256	264.03	13.5	4.7	212.84
	256	1056.12	13.7	9.9	449.32

TABLE 2. Sensitivity of the algorithm to Reynolds number. Here ASM overlap $\delta = 8$ and $\nu_s = 0.30$.

addition, we are considering a non-Newtonian fluid model for the blood, a multilevel preconditioner to improve scaling, and a possible extension to three dimensions.

REFERENCES

[1] S. Balay, K. Buschelman, V. Eijkhout, W. D. Gropp, D. Kaushik, M. G. Knepley, L. C. McInnes, B. F. Smith, and H. Zhang. PETSc users manual. Technical Report ANL-95/11 - Revision 2.1.5, Argonne National Laboratory, 2004.

[2] S. Balay, K. Buschelman, W. D. Gropp, D. Kaushik, M. G. Knepley, L. C. McInnes, B. F. Smith, and H. Zhang. PETSc Web page, 2001. http://www.mcs.anl.gov/petsc.

[3] Y. Bazilevs, V. Calo, Y. Zhang, and T. Hughes. Isogeometric fluid-structure interaction analysis with applications to arterial blood flow. *Computational Mechanics*, 38:310–322, 2006.

[4] J. Donea, A. Huerta, J.-P. Ponthot, and A. Rodríguez-Ferran. Arbitrary Lagrangian-Eulerian methods. In E. Stein, R. de Borst, and T. J. Hughes, editors, *Encyclopedia of Computational Mechanics*, volume 1, pages 1–25. Wiley, 2004.

unknowns	np	ν	GMRES	Newton	time
	256	0.30	13.6	4.8	138.65
	256	0.40	15.1	5.0	147.92
$2.1 \cdot 10^6$	256	0.49	27.9	7.3	229.27
	512	0.30	13.6	4.8	100.59
	512	0.40	15.5	5.0	104.23
	512	0.49	31.1	7.3	162.92
	256	0.30	14.0	4.7	180.65
	256	0.40	15.6	4.8	185.84
$2.6 \cdot 10^6$	256	0.49	27.9	7.3	298.67
	512	0.30	16.1	4.6	81.22
	512	0.40	17.9	4.8	86.86
	512	0.49	37.2	7.3	145.43

TABLE 3. Sensitivity of the algorithm to Poisson ratio ν_s. Here ASM overlap $\delta = 6$ and Reynolds number = 33.00.

[5] A. Figueroa, I. Vignon-Clementel, K. Jansen, T. Hughes, and C. Taylor. Simulation of blood flow and vessel deformation in three-dimensional, patient-specific models of the cardiovascular system using a novel method for fluid-solid interactions. *Fluid Structure Interaction and Moving Boundary Problems*, 1:143–152, 2005.

[6] C. A. Figueroa, I. E. Vignon-Clementel, K. E. Jansen, T. J. Hughes, and C. A. Taylor. A coupled momentum method for modeling blood flow in three-dimensional deformable arteries. *Computer Methods in Applied Mechanics and Engineering*, 195:5685–5706, 2006.

[7] L. Formaggia, J. Gerbeau, F. Nobile, and A. Quarteroni. On the coupling of 3D and 1D Navier-Stokes equations for flow problems in compliant vessels. *Computer Methods in Applied Mechanics and Engineering*, 191:561–582, 2001.

[8] P. Gresho and R. Sani. *Incompressible Flow and the Finite Element Method*. Wiley, New York, 1998.

[9] T. J. Hughes. *The Finite Element Method: linear static and dynamic finite element analysis*. Dover, 2000.

[10] K. S. Hunter, C. J. Lanning, S.-Y. J. Chen, Y. Zhang, R. Garg, D. D. Ivy, and R. Shandas. Simulation so f congenital septal defect closure and reactivity testing in patient-specific models of the pediatric pulmonary vasculature: a 3D numerical study with fluid-structure interaction. *Journal of Biomechanical Engineering*, 128:564–572, 2006.

[11] E. Kuhl, S. Hulshoff, and R. de Borst. An arbitrary Lagrangian Eulerian finite-element approach for fluid-structure interaction phenomena. *International Journal for Numerical Methods in Engineering*, 57:117–142, 2003.

[12] C. J. Murray and A. D. Lopez. Mortality by cause for eight regions of the world: Global Burden of Disease study. *Lancet*, 349:1269–1276, 1997.

[13] F. Nobile. *Numerical approximation of fluid-structure interaction problems with application to haemodynamics*. PhD thesis, École Polytechnique Fédérale de Lausanne, 2001.

[14] S. Ovtchinnikov, F. Dobrian, X.-C. Cai, and D. Keyes. Domain-decomposed fully coupled implicit methods for a magnetohydrodynamics problem. In O. B. Widlund and D. E. Keyes, editors, *Domain Decomposition Methods in Science and Engineering XVI*, pages 333–340. Springer, 2007.

[15] L. F. Pavarino and E. Zampieri. Overlapping Schwarz and spectral element methods for linear elasticity and elastic waves. *Journal of Scientific Computing*, 27:51–73, 2006.

[16] F. van de Vosse, J. D. Hart, C. V. Oijen, D. Bessems, T. Gunther, A. Segal, B. Wolters, J. Stijnen, and F. Baaijens. Finite-element-based computational methods for cardiovascular fluid-structure interaction. *Journal of Engineering Mathematics*, 47:335–368, 2003.

[17] I. E. Vignon-Clementel, C. A. Figueroa, K. E. Jansen, and C. A. Taylor. Outflow boundary conditions for three-dimensional finite element modeling of blood flow and pressure in arteries. *Computer Methods in Applied Mechanics and Engineering*, 195:3776–3796, 2006.